The Astrophysical Journal, 598:288–300, 2003 November 20

STAR FORMATION AND X-RAY EMISSION IN DISTANT STAR-FORMING GALAXIES[1]

Judith G. Cohen[2]

Received 2003 May 7; accepted 2003 July 30

ABSTRACT

About 45% of the point sources detected in the 2 Ms *Chandra* exposure of the Hubble Deep Field–North (HDF-N) can be matched with moderately bright galaxies with $z < 1.4$ that have been studied by the Caltech Faint Galaxy Redshift Survey. Although the optical spectra of these galaxies appear normal, based on their X-ray properties ~20% of them appear to contain weak active galactic nuclei (AGNs). More than 90% of the X-ray photons detected by *Chandra* from galaxies within the redshift regime $0.4 < z < 1.1$ are powered by accretion onto massive black holes. For the sample of galaxies in common, we use their emitted luminosity in the 3727 Å line of [O II] to estimate their star formation rates (SFRs). The X-ray–emitting galaxies are not those with the highest rest-frame equivalent width in this emission line, but rather are among those with the highest SFRs. With SFRs corrected for inclination effects, the distant galaxies show an L_X-SFR relationship that is comparable to that of local galaxies. The HDF sample has a significantly higher median SFR and median SFR/galaxy stellar mass than does a sample of local star-forming galaxies. We demonstrate that the observed SFR for most of the galaxies at $z \sim 1$ in the HDF sample, if maintained as constant over their ages, suffices to produce the stellar mass observed in these galaxies. A rise in SFR at still earlier times is not required. We provide further evidence to support the conclusion that, once AGNs are eliminated, X-ray emission in these distant star-forming galaxies is related to the SFR through the same physical mechanisms that prevail locally.

Subject headings: galaxies: ISM — galaxies: starburst — X-rays: galaxies

1. INTRODUCTION

The release of the point-source catalogs for the 2 Ms exposure of the *Chandra* Deep Field–North (CDF-N) by Alexander et al. (2003) represents a milestone for astronomy. The large collecting area and high spatial resolution of *Chandra* have, with this extremely long exposure time, achieved sufficient sensitivity to detect the population of distant normal galaxies. Much previous work on the optical counterparts to the *Chandra* detections in the region of the Hubble Deep Field (HDF), such as that of Barger et al. (2002, 2003), has focused on the optically faintest counterparts of X-ray sources, in efforts to find very distant galaxies, heavily obscured, distant active galactic nuclei (AGNs), etc. In this paper we address the origin of the X-ray emission from the *Chandra* sources with optical counterparts corresponding to "faint" field galaxies, using material from the Caltech Faint Galaxy Redshift Survey (CFGRS), described in Cohen et al. (2000) and Cohen (2001).

The CFGRS was carried out in the region of the Hubble Deep Field–North (HDF-N, hereafter simply HDF; Williams et al. 1996), which is included within the larger area of the CDF-N. Our redshift survey there achieves very high completeness to a deep limiting magnitude. The survey sample was selected based on the four-color optical and infrared photometric catalogs of Hogg et al. (2000) and covers the area within a diameter of 8′ centered on the HDF. Objects were observed spectroscopically using LRIS at the 10 m Keck Telescope (Oke et al. 1995), irrespective of morphology, to include all AGNs, QSOs, and other possible extragalactic objects that might appear stellar. Our composite catalog for the region of the HDF contains ≈595 galaxies with $z < 1.5$ and includes the work of the Caltech and Hawaii groups through 1999 (see Cohen et al. 1996 for a progress report as of that date) and the subsequent work of the Caltech group, as well as the published data from Phillips et al. (1997) (from the Lick Deep Group) and five unpublished redshifts from C. Steidel. Our composite catalog contains redshifts for more than 93% of the sample, to a limiting magnitude of $R < 24$ in the HDF itself and to $R < 23.5$ in the flanking fields.

Of the 503 *Chandra* sources securely detected by Alexander et al. (2003), 149 are within the 8′ diameter area covered by the CFGRS. We adopt a requirement that the X-ray and optical positions must match to within a tolerance of 1″.5, based on the astrometric accuracy of the *Chandra* and Hogg et al. (2000) catalogs. We then find that 67 of these X-ray point sources can be matched with galaxies with $z < 1.4$ in this field.[3] Hence, about 45% of the very deep X-ray detections reported by Alexander et al. (2003) arise from galaxies at intermediate redshifts that appear from their optical spectra to be normal. In the present paper, we compare the X-ray emission detected by *Chandra* with the star formation rates (SFRs) inferred from the [O II] emission lines of these galaxies. As in earlier papers in this series, we adopt the cosmology $H_0 = 60$ km s^{-1} Mpc^{-1}, $\Omega_M = 0.3$, and $\Omega_\Lambda = 0$. Over the redshift interval of most interest, a flat universe with $\Omega_\Lambda = 0.7$ and a Hubble constant of $H_0 = 67$ km s^{-1} Mpc^{-1} gives galaxy luminosities very close to those used below.

[1] Based in part on observations obtained at the W. M. Keck Observatory, which is operated jointly by the California Institute of Technology, the University of California, and the National Aeronautics and Space Administration.

[2] Palomar Observatory, MS 105-24, California Institute of Technology, Pasadena, CA 91125; jlc@astro.caltech.edu.

[3] One additional *Chandra* point source is matched with a Galactic M dwarf star, and one other is matched with a high-redshift QSO in this field.

2. ELIMINATING AGNs FROM THE SAMPLE

The mechanisms giving rise to the X-ray emission of local star-forming galaxies, reviewed by Fabbiano (1989), are a composite of emission from the interstellar medium (ISM), from stellar sources (predominantly X-ray binaries), from supernova remnants, and possibly from a nuclear AGN. With the aid of *Chandra*'s high spatial resolution, separation of these components in nearby galaxies becomes feasible; see, e.g., Zezas & Fabbiano (2002) for the Antennae galaxy. In nearby galaxies with high current SFRs, X-ray binaries provide about half of the flux in the full *Chandra* band. The hot components of the ISM, which contribute most of the remaining flux, can also be studied in detail with *Chandra*. The superbubbles, whose evolution was followed by Tenorio-Tagle et al. (1999), can be resolved, galactic winds can be detected, and the metallicity of the gas within them determined (see, e.g., Martin, Kobulnicky, & Heckman 2002). In addition, the sensitivity of *XMM* permits detection of a complex array of lines and precision spectral fitting for X-ray–bright nearby galaxies, such as M82 (Read & Stevens 2002). While Hornschemeier et al. (2003) have detected off-nuclear luminous X-ray sources in galaxies to $z \sim 0.1$ in the HDF, none of this richness can be achieved at present for the distant galaxies in our sample.

The variation of the X-ray emission from nuclear sources, particularly given the low spatial resolution of early X-ray images, can be explained by either the X-ray burst or the AGN hypothesis. (See, e.g., Ptak & Griffiths 1999, for M982.) For M51, however, the detection of optical emission lines characteristic of a central, weak, low-luminosity AGN by Ho, Filippenko, & Sargent (1997) is definitive proof that weak AGNs may be present even in these heavily star-forming galaxies; they find such weak AGNs in a high fraction of local galaxies. But the nucleus of M51 contributes only 12% of its total full-band *Chandra* luminosity; the bulk of its X-ray emission comes from the extended and stellar sources (Terashima & Wilson 2003).

We consider here only those galaxies in the region of the HDF whose optical spectra show signs of moderate-to-strong current star formation, i.e., galaxies with easily detected optical emission lines. These have been assigned galaxy spectral classes in the CFGRS catalog using the Cohen et al. (1999) definitions of $\mathscr{I}$ (moderately strong emission lines with detectable absorption lines as well) and $\mathscr{E}$ (very strong emission lines). Two broad-lined AGNs have been culled out of the sample of 595 galaxies; both of these have very high X-ray luminosities from the *Chandra* data. However, elimination of narrow-lined AGNs based solely on their optical spectra is difficult as, for the higher redshift galaxies considered here, none of the key diagnostic features falls within the wavelength coverage of the available optical spectra. Furthermore, the light of any nuclear AGNs will be diluted in such distant galaxies by the large metric aperture used for ground-based spectroscopic observations (Moran, Filippenko, & Chornock 2002).

In the local universe, the mass of a nuclear AGN (i.e., a black hole) depends primarily on the mass of the stellar bulge component of the host galaxy (Ferrarese & Merritt 2000). The luminosity of the star-forming galaxies in the HDF is, for a given SFR, in the mean considerably higher than that for local star-forming galaxies (Cowie et al. 1996; Cohen 2001). Furthermore, at high redshift, there may be more gas to power the central source. Hence, we may expect the effect of contributions from AGNs to be more important in the HDF than in local samples.

There is a well-established relationship between the far-IR luminosity and the radio luminosity (see, e.g., Condon 1992) among local star-forming galaxies, whose origin was discussed by Bell (2003). Garrett (2002) explored this relation at moderate redshifts by comparing the far-IR (from *ISO*) and radio emission of 20 galaxies from the CFGRS in the HDF with that of a local sample. He found that the correlation between far-IR and radio emission established in local star-forming galaxies continues to apply out to $z \sim 1.3$. Deviations of excess radio luminosity from such a well-defined relationship presumably imply the presence of an AGN. However, the far-IR data in the region of the HDF (from *ISO*; Aussel et al. 1999) are quite limited, both in depth and in size of field, and are insufficient for our purposes. Until *SIRTF* data are in hand, we cannot use this approach to test for AGNs.

To shed light on the possible presence of AGNs in our HDF samples, we build on the work of Grimm, Gilfanov, & Sunyaev (2003), who studied a small sample of galaxies in the HDF with both radio and *Chandra* observations and with redshifts from the CFGRS. They, too, suggested that the local relations apply to their HDF sample. We therefore construct the set of objects that are included in each of the *Chandra* point-source catalog, the CFGRS (for redshifts), and the Very Large Array (VLA)[4] database for the HDF of Richards et al. (1998) and Richards (2000). As one step toward eliminating AGNs, we omit all sources for which the *Chandra* spectral index is negative (i.e., very hard sources). Galaxies that are in close pairs of comparable luminosity in the CFGRS were included only if it was clear to which component the *Chandra* detection should be assigned. If not, such galaxies were ignored. Eleven galaxies meet these criteria. These galaxies are indicated in Table 1, and some median properties of the sample are given in Table 2.

Both the X-ray and the radio emission arising from star-forming galaxies are essentially free of reddening effects and hence should be tightly coupled. Figure 1 shows the resulting $L_{1.4\,\mathrm{GHz}}$ versus L_{X} for the 11 sources in common. A k-correction for the radio has been used, since all but one of the galaxies have measured radio spectral indices, but none was used in calculating the X-ray luminosity. Power-law spectral energy distributions (SEDs), in the form of $f(\nu) \propto \nu^{-\alpha}$, have k-corrections for luminosities $\nu L(\nu)$ of $(1+z)^{\alpha-1}$. For a slope α between 1 and 2, typical of these X-ray sources, the k-correction has a total range from 0.0 to 0.3 dex for $z = 0$–1.

Most of the points define a tight line, as expected, but two of them, F36422_1545[5] and F36517_1220, lie significantly above it. Luminous, discrete, nonnuclear X-ray sources, also known as ULX sources, found in local galaxies are reviewed by Makishima et al. (2000); the most luminous of these reach $L_{\mathrm{X}} \geq 4 \times 10^{32}$ W in M51 (Terashima & Wilson 2003). These two HDF galaxies have luminosities far higher than any local ULX and presumably contain luminous AGNs. The redshift of F36422_1545 is $z = 0.857$, so the

[4] The VLA is a facility of the National Radio Astronomy Observatory (NRAO). The NRAO is a facility of the National Science Foundation operated under cooperative agreement by Associated Universities, Inc.

[5] Galaxy names are based on the J2000.0 coordinates of the object; e.g., an object at 12 12 34.5, +62 56 43 is identified as F12345_5643.

TABLE 1

STAR FORMATION RATES FOR GALAXIES IN THE HDF-N

ID	z	$W_\lambda(3727)$[a] (Å)	$\log[\mathrm{SFR}^i(3727)]$ ($M_\odot\ \mathrm{yr}^{-1}$)	Radio/VLA[b]
		$\mathscr{E}$ Galaxies		
F36194_1252	0.474	14.1 ± 1.5	$0.74^{+0.10}_{-0.14}$	Y
F36199_1251	0.695	55.7 ± 5.0	$0.86^{+0.10}_{-0.14}$	
F36211_1208	0.841	15.3 ± 2.0	$1.18^{+0.11}_{-0.15}$	
F36246_1111[c]	0.748	6.9 ± 2.0	$0.20^{+0.14}_{-0.21}$	
F36273_1258	1.221	28.4 ± 7.1	$1.34^{+0.13}_{-0.19}$	
F36312_1236	0.455	75.5 ± 7.6	$0.99^{+0.10}_{-0.13}$	
F36332_1134	0.080	33.0 ± 3.0	-0.42 ± 0.12	
F36336_1005[c]	1.015	40.7 ± 10.0	$1.30^{+0.13}_{-0.19}$	
F36346_1241[c]	1.219	111.2 ± 33.3	$1.60^{+0.14}_{-0.21}$	Y
F36348_1628	0.847	11.7 ± 2.2	$0.56^{+0.12}_{-0.17}$	
F36363_1320	0.680	40.9 ± 8.2	0.66 ± 0.12	
F36389_1257	1.127	6.8 ± 2.0	$0.67^{+0.14}_{-0.23}$	
F36440_1250	0.557	25.3 ± 7.6	$0.95^{+0.11}_{-0.15}$	Y
F36470_1237	0.321	28.6 ± 4.3	$0.30^{+0.11}_{-0.15}$	
F36517_1220	0.401	36.6 ± 7.3	$0.90^{+0.12}_{-0.17}$	Y
F36521_1457	0.358	46.9 ± 4.7	$0.60^{+0.10}_{-0.15}$	
F36527_1355	1.355	$114.0^{+28.5}_{-57}$	$2.25^{+0.13}_{-0.36}$	
F36534_1140	1.275	$54.7^{+13.7}_{-27.4}$	$1.11^{+0.13}_{-0.34}$	Y
F36573_1026	0.847	$20.1^{+5.0}_{-10.1}$	$0.29^{+0.13}_{-0.36}$	
F36599_1450	0.762	35.0 ± 5.3	$1.47^{+0.11}_{-0.15}$	Y
F37004_1617[c]	0.913	34.2 ± 5.1	$0.91^{+0.11}_{-0.15}$	
F37144_1221	1.084	$22.8^{+5.7}_{-11.4}$	$0.65^{+0.13}_{-0.36}$	
		$\mathscr{I}$ Galaxies		
F36230_1346	0.485	23.4 ± 2.3	$0.88^{+0.10}_{-0.14}$	
F36345_1213	1.015	14.1 ± 1.4	$1.32^{+0.10}_{-0.14}$	Y
F36397_1010	0.509	14.0 ± 2.0	0.23 ± 0.12	
F36399_1250[c]	0.848	17.2 ± 1.7	$0.93^{+0.10}_{-0.14}$	
F36422_1545	0.857	13.0 ± 2.8	$1.18^{+0.12}_{-0.17}$	Y
F36431_1109[c]	0.297	$13.5^{+6.3}_{-3.4}$	-0.75 ± 0.20	
F36481_1309	0.476	21.8 ± 2.2	$0.86^{+0.11}_{-0.15}$	
F36509_1031	0.410	10.4 ± 1.6	$0.33^{+0.11}_{-0.15}$	Y
F36588_1638	0.299	11.3 ± 1.7	$0.57^{+0.11}_{-0.15}$	
F36588_1435	0.678	4.7 ± 1.4	$0.49^{+0.14}_{-0.21}$	
F37020_1123	0.136	22.1 ± 3.3	$0.20^{+0.10}_{-0.14}$	
F37027_1543	0.514	8.3 ± 1.2	$0.71^{+0.11}_{-0.15}$	
F37046_1429	0.561	8.8 ± 1.8	$0.52^{+0.12}_{-0.17}$	
F37058_1154	0.904	23.3 ± 4.7	$1.26^{+0.11}_{-0.17}$	Y
F37083_1056	0.423	34.5 ± 6.9	$1.39^{+0.12}_{-0.17}$	Y
F37138_1424	0.475	34.2 ± 5.1	$0.79^{+0.11}_{-0.15}$	

[a] Rest-frame equivalent width of the 3727 Å emission line.
[b] These galaxies have been detected with the VLA (Richards et al. 1998; Richards 2000).
[c] No axis ratio could be measured for this galaxy.

TABLE 2

MEDIANS OF SAMPLES

Sample	Galaxies	z	$\mathrm{SFR}^i(\mathrm{H}\alpha)$ ($M_\odot\ \mathrm{yr}^{-1}$)	$\mathrm{SFR}^i(3727)$ ($M_\odot\ \mathrm{yr}^{-1}$)	$\log M$[a] ($M_\odot$)	$\mathrm{SFR}^i/10^{11}\ M_\odot\,(\mathrm{H}\alpha)$ ($M_\odot\ \mathrm{yr}^{-1}$)	$\mathrm{SFR}^i/10^{11}\ M_\odot\,(3727)$ ($M_\odot\ \mathrm{yr}^{-1}$)
			HDF Sample				
X-ray+radio+CFGRS[b]	11	0.76	...	15.1	11.09	...	13.8
X-ray+CFGRS/$\mathscr{E}$	22	0.84	...	7.6	10.71	...	17.8
X-ray+CFGRS/$\mathscr{I}$	16	0.49	...	5.6	10.88	...	5.4
			Local Galaxies				
Local calibrators	14	0.00	2.9	...	10.75	7.2	...

[a] Log of the stellar mass inferred from the luminosity at rest-frame K.
[b] Only galaxies with optical emission lines are included.

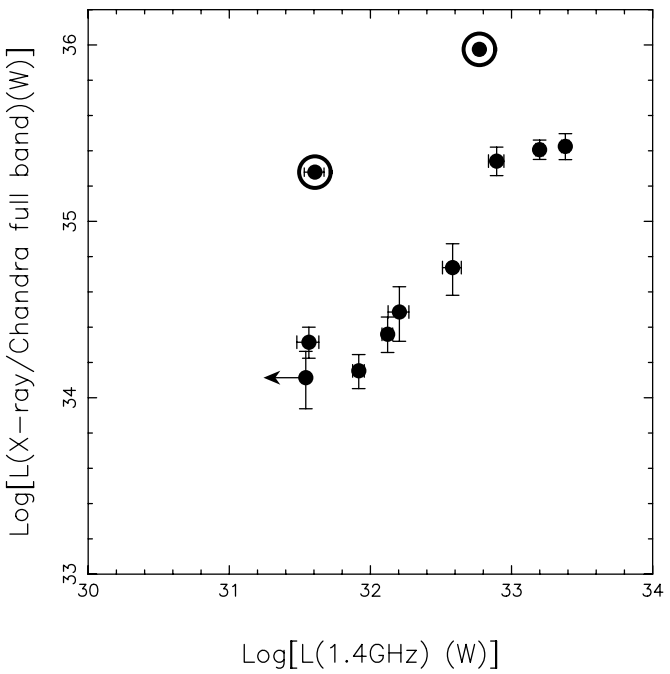

FIG. 1.—Total X-ray luminosity over the full *Chandra* band as a function of the radio luminosity at 1.4 GHz from Richards et al. (1998) and Richards (2000), for a sample of 11 star-forming galaxies in the region of the HDF that appear as point sources in the *Chandra* catalog of Alexander et al. (2003), are detected with the VLA, have redshifts from the CFGRS, and meet several other criteria described in the text. The two suspected AGNs are circled.

region of Hβ is too far to the red to be accessible. The more modest redshift of F36517_1220 ($z = 0.401$) permits an examination of the rest frame 5000 Å region, although Hα is inaccessible. This means that the conventional AGN diagnostics used in the optical spectroscopy of Baldwin, Phillips, & Terlevich (1981) and Veilleux & Osterbrock (1987) are out of reach. Judging by the more limited test of line strength ratios, avoiding the Hα region, introduced by Rola, Terlevich, & Terlevich (1997), F36517_1220 is a normal star-forming galaxy. Reconciliation of these conflicting claims is possible with the conjecture of Moran et al. (2002) regarding the importance of aperture effects on the detection of AGNs at high redshift from optical spectra.

Figure 2 shows the full-band *Chandra* counts as a function of the galaxy redshift for the sample of star-forming galaxies in the region of the HDF of this paper. A detailed description of the sample selection is given in § 4. We ascribe the sprinkling of galaxies along the bottom of this figure to X-ray emission associated with normal star formation. The two suspected AGNs isolated in Figure 1 are circled, and they are among the most discrepant galaxies in Figure 2. There are two galaxies in our sample with full-band *Chandra* detections that exceed 1000, while the two broad-lined AGNs that were eliminated from the sample have full-band *Chandra* detections in excess of 2000 counts.

If we assume that all galaxies with full-band *Chandra* counts in excess of 100 contain an AGN, then there are two broad-lined and eight narrow-lined AGNs in our sample, of which only the two broad-lined galaxies were picked out from their optical spectra as AGNs. The fraction of the total *Chandra*-detected flux originating from accretion onto a massive black hole is ~93%. The much more numerous normal star-forming galaxies contribute very little to the total X-ray luminosity density.

There are, in addition, five or six additional galaxies in this sample of 38 that are clearly discrepant, with excess X-ray flux, although their optical spectra appear normal. Only one of these six galaxies has a radio detection. These, too, presumably have weak AGNs.

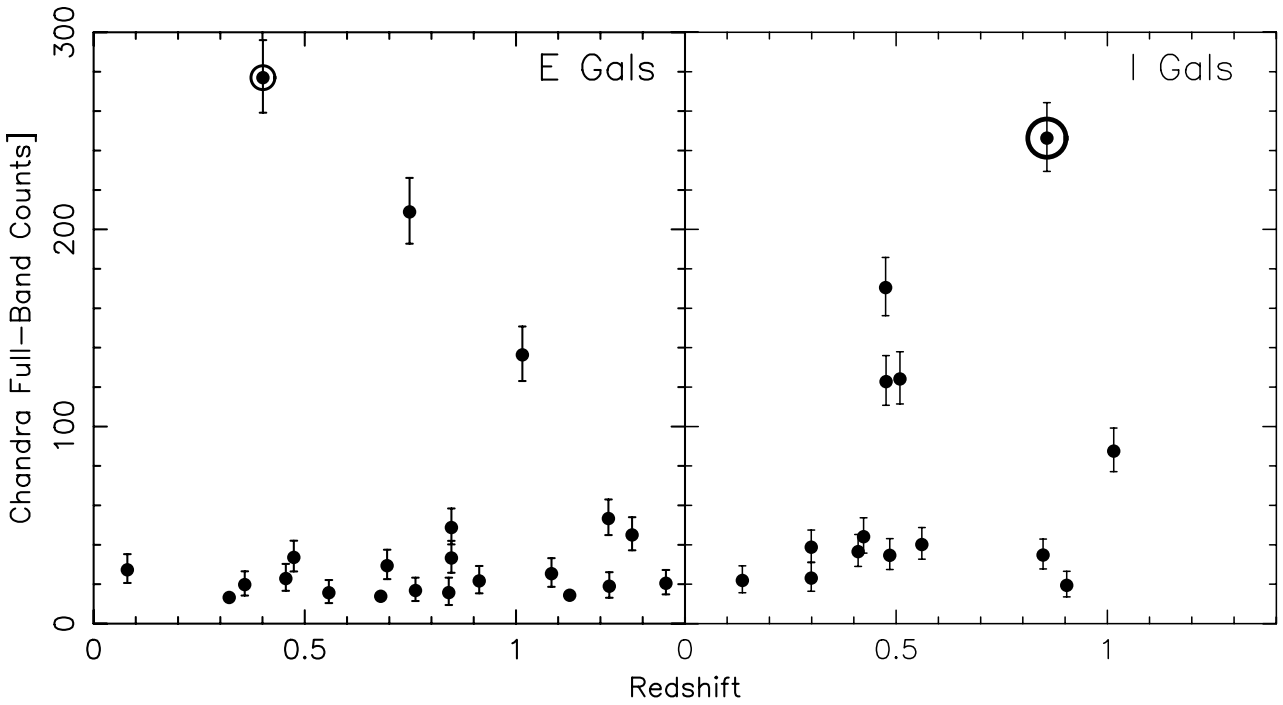

FIG. 2.—Detected counts over the full *Chandra* band as a function of the galaxy redshift for the 22 *E* galaxies (*left*) and the 16 *I* galaxies (*right*). Two of the *I* galaxies have more than 1000 detected *Chandra* full-band counts and hence do not appear in this plot.

To within the small-number statistics of the present sample, we therefore assert that about 20% of the spectroscopically normal, high-luminosity, star-forming galaxies in the HDF have nuclear AGNs that contribute substantially to their total X-ray fluxes. Huchra & Burg (1992) give the frequency of Seyfert I and Seyfert II galaxies in the CfA Redshift Survey of the local universe, while Ho et al. (1997) have done so for AGNs reaching to much lower luminosities. Both the AGN luminosity and the very rough AGN fraction derived above for our sample lie between these local determinations. Kobulnicky et al. (2003) find that 15% of their sample of 66 star-forming galaxies with $0.26 < z < 0.82$ in the Groth strip are probably narrow-lined AGNs.

L_X, L_{radio}, and L_{FIR} are to first order independent of internal reddening within the galaxy, and hence these correlations, including that shown in Figure 1 for a sample of galaxies in the region of the HDF, have quite small dispersions, both among local galaxies and in the HDF using the CFGRS database, ignoring the obvious occasional outliers, which we presume to be AGNs. The underlying variable driving these correlations is widely assumed to be the SFR.

3. THE SAMPLE OF LOCAL CALIBRATORS

We first create a sample of local star-forming/starburst galaxies for comparison with our sample of much more distant galaxies in the region of the HDF. Their properties and the references from which their X-ray luminosities and Hα fluxes were taken are given in Table 3. We have modified the published data to correspond to $H_0 = 70$ km s^{-1} Mpc^{-1} and have removed the Galactic extinction, using the maps of Schlegel, Finkbeiner, & Davis (1998), when necessary. We correct the SFR for inclination effects; the result is denoted SFR^i. We take axis ratios for our sample of local calibrators from the Two Micron All-Sky Survey (2MASS) Large Galaxy Atlas (Jarrett et al. 2003) or, if necessary, measure them from NED images. We apply a correction of the form $\Delta(\mathrm{mag}) = \gamma \log(b/a)$ and adopt $\gamma(\mathrm{H}\alpha) = 1.3$ (Tully et al. 1998). This does not remove the reddening experienced by a face-on disk galaxy.

We have also applied small corrections to total galaxy X-ray fluxes taken from the catalog of galaxy observations with the *Einstein* satellite of Fabbiano et al. (1992), given over the regime 0.2–4.0 keV, to cover the full *Chandra* bandpass. The observed fluxes in the optical emission lines for these local galaxies have in most cases been measured through apertures large enough to encompass the entire galaxy, except for the data taken from Calzetti et al. (1995). Substantial aperture corrections for this data set are required and were calculated using images from NED, under the assumption that the spatial distribution of the flux in the emission line is the same as that of a nearby broad-band, continuum-dominated filter. The Hα fluxes from Calzetti et al. (1995) as published are corrected for the internal reddening of the galaxy, and this was backed out prior to use.

Our local sample of star-forming galaxies was selected based on our ability to locate the required observational material in the literature. Few surveys of large-aperture observations of nearby galaxies in the optical emission lines are available. We began with the sample of Bell & Kennicutt (2001) and tried to locate the requisite X-ray emission for the galaxies in their sample with substantial SFRs. A special effort had to be made to find suitable local galaxies with high SFRs; such galaxies are rare in the local universe. The two local galaxies with the highest SFRs are at distances D of 56 and 78 Mpc, while all the others have $D < 20$ Mpc, and 9 of the 14 have $D \leq 10$ Mpc. Kauffmann et al. (2003) have analyzed a large sample of galaxies from the Sloan Digital Sky Survey (SDSS) and find that the percentage of local galaxies with signs of a recent or ongoing starburst decreases rapidly as the luminosity increases, so our difficulty in finding luminous local galaxies with high SFRs is not surprising.

These local galaxies, with Hα used as the diagnostic for star formation, are indicated by filled circles in Figure 3; for $(B-V)_0 > 0.6$, they are indicated by asterisks. A

TABLE 3
LOCAL CALIBRATING GALAXIES

ID	$\log L_X$ (W)	$\log M$[a] ($M_\odot$)	$\log[\mathrm{SFR}^i(\mathrm{H}\alpha)/10^{11}\ M_\odot]$ ($M_\odot$ yr^{-1})	$\log[\mathrm{SFR}^i(3727)]$ ($M_\odot$ yr^{-1})	References	
					X-Ray	Optical
NGC 253	33.11	10.57	0.58	...	1	2
NGC 628	32.78	10.51	0.55	...	1	2
NGC 891	32.99	10.86	0.19	...	3	2
NGC 1614	34.62	11.15	1.58	...	3	4
NGC 3031 (M81)	33.15	10.75	0.20	...	1	2
NGC 3034 (M82)	33.38	10.42	1.05	−0.24	5	2
NGC 3256	35.00	11.22	1.61	...	6, 7	4
NGC 3310	33.58	10.08	1.61	0.67	1	2
NGC 4038[b]	34.08	10.87	1.13	...	8	2, 9
NGC 4321 (M100)	33.74	11.00	0.55	...	10	2
NGC 4449	32.45	9.41	1.58	−0.12	1, 11	2
NGC 4631	33.26	10.51	1.20	0.49	1	2
NGC 5194 (M51)	32.92	10.77	0.74	−0.47	1, 12	2
NGC 5236 (M83)	32.68	10.53	0.96	...	13	2

[a] Log of the stellar mass inferred from the luminosity at rest-frame K.
[b] Also known as the Antennae galaxy.

REFERENCES.—(1) Fabbiano, Kim & Trinchieri 1992; (2) Bell & Kennicutt 2001; (3) Ueda et al. 2001; (4) Calzetti, Kinney, & Storchi-Bergmann 1994; Calzetti et al. 1995; (5) Ptak & Griffiths 1999; (6) Lira et al. 2002; (7) Moran, Lehnert, & Helfand 1999; (8) Fabbiano, Zezas, & Murray 2001; (9) Young et al. 1996; (10) Immler, Pietsch, & Aschenbach 1998; (11) Vogler & Pietsch 1997; (12) Terashima & Wilson 2001); (13) Okada, Mitsuda, & Dotani 1997.

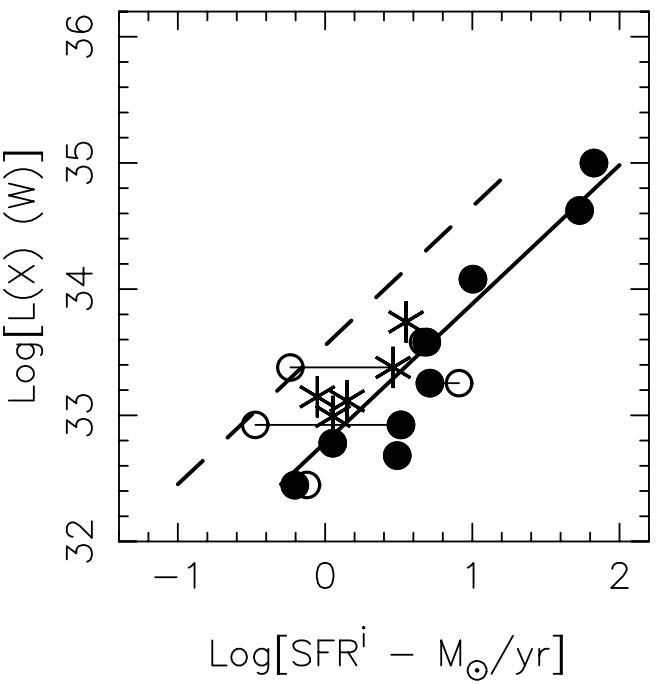

FIG. 3.—Total X-ray luminosity over the full *Chandra* band as a function of the SFR deduced from the Hα flux corrected for inclination effects, for the sample of 14 local calibrating star-forming galaxies. Filled circles represent SFRs derived from Hα luminosities for galaxies with $(B-V)_0 > 0.6$, asterisks those of the redder star-forming galaxies, and open circles those using the 3727 Å emission line of [O II] as a diagnostic. Thin horizontal lines connect galaxies with measurements using both diagnostic lines. The thick solid line denotes the least-squares fit. The dashed line is offset in SFR^i from that by −0.7 dex, corresponding to the maximum offset seen for $\mathrm{SFR}^i(3727)$ with respect to $\mathrm{SFR}^i(\mathrm{H}\alpha)$.

least-squares linear fit to the 14 points is shown by the thick solid line and has the form

$$\log L_X = 32.783 \pm 0.115 + (1.100 \pm 0.140) \log\left[\mathrm{SFR}^i(\mathrm{H}\alpha)\right] ,$$

with σ about this fit of 0.31 dex. The scatter would be noticeably larger if the inclination corrections were not used. Several smaller sources contribute to the remaining scatter in the relation between L_X and $\mathrm{SFR}^i(\mathrm{H}\alpha)$. They include the small corrections applied to intercompare observations made with three different X-ray telescopes (*Chandra*, *ASCA*, and *Einstein*), ignoring the X-ray *k*-corrections and, most importantly, ignoring reddening differences between galaxies in the local sample after they have been corrected to face-on. Table 4 gives an estimate of the contribution of each of these terms to the observed σ. In addition, at the lowest L_X for these nearby galaxies, the number of detected discrete, nonnuclear X-ray sources, presumably various types of luminous X-ray binaries, that may contribute an amount equal to the extended emission becomes fairly small, and Poisson statistics may become important.

We are using the 3727 Å emission line of [O II] as our diagnostic of SFR for our sample of distant galaxies in the region of the HDF. However, among local galaxies there are fewer measurements of the observed integrated flux in the 3727 Å emission line of [O II] than there are for Hα. This is presumably because the [O II] emission line is less dominant in its spectral region than is Hα. Also, the adjacent continuum is chopped up by strong absorption features there; hence, narrowband imaging is not feasible.

The major surveys for the strength of the 3727 Å emission line of [O II] among local galaxies are those of Gallagher, Bushouse, & Hunter (1989) and Kennicutt (1992). Substantial aperture corrections are required for the former, while for the latter, the observed [O II] line fluxes are given with respect to the observed Hα flux. We were able to locate

TABLE 4

CONTRIBUTIONS TO THE SCATTER OF SFR^i VERSUS L_X

Concern	$\sigma \log[\mathrm{SFR}^i(3727)]$ (dex)	$\sigma \log[\mathrm{SFR}^i(\mathrm{H}\alpha)]$ (dex)
Optical		
$\sigma[E(B-V)] = 0.2$ mag	0.4	0.2
O abundance	0.1[a]	0.0
O excitation	0.2	0.0
Optical flux uncertainty	0.15	0.1
Optical aperture correction	0.05[b]	...
Inclination correction uncertainty	0.1	0.05
X-Ray		
No X-ray *k*-correction	0.1	0.1
Conversion to *Chandra*[c]	0.05	0.05
Total σ		
Predicted total σ[d]	0.51	0.26
Observed σ	...	0.31

[a] Calculated from the fit of [O II] 3727/Hα to a sample of local galaxies of known O/H by Jansen, Franx, & Fabricant 2001.

[b] The spectra are generally obtained through a slit that is too small to pass all the light from the galaxy. See the text for how this is taken into account. This term is the uncertainty in the correction.

[c] Conversion between *ASCA*, *Einstein*, and *Chandra* full-band fluxes.

[d] This is the sum in quadrature of the terms listed above.

suitable measurements for only five of the galaxies in the local sample, all from Kennicutt (1992). The resulting deduced SFR^i values, using the calibration of Kennicutt (1998), are shown in Figure 3 as open circles. Thin horizontal lines connect the Hα and [O II] SFRs. This offset in SFR^i represents mainly the difference $\Delta(A)$ between $A(\mathrm{H}\alpha)$ and $A(3727)$, where $A(\lambda)$ is the total absorption for the integrated light of each of the calibrating galaxies (corrected to face-on).

Reddening curves for galaxies are quite controversial (Calzetti 1999), but most of the disagreement lies within the rest-frame UV, which we do not use. We therefore adopt $A(\lambda)/A(V)$ of Schlegel et al. (1998), so $\Delta(A) = 2.26E(B-V)$ mag. The differential extinction appears small for three of the galaxies and much larger for NGC 3034 and NGC 5194. The dashed line shows the fit to Hα translated by -0.7 dex in $\log SFR^i$ so as to fit through the values of these last two galaxies, which are among the more reddened of the local calibrators. Note that $\Delta(A) = 0.7$ dex $\equiv 1.75$ mag corresponds to a total reddening for a face-on galaxy of $E(B-V) = 0.8$ mag. This is not unreasonable for star-forming galaxies; the references quoted in Table 3 often ascribe $A(\mathrm{H}\alpha) = 1.0$–1.5 mag [equivalent to $E(B-V) = 0.4$–0.6 mag] to the individual galaxies or the sample of galaxies studied in each case; see also Kennicutt (1983) and Cohen (2001).

There are many more surveys of emission lines in local star-forming galaxies using small apertures, which concentrate on the galactic nucleus, e.g., McQuade, Calzetti, & Kinney (1995) and Storchi-Bergmann, Kinney, & Challis (1995). We, however, rely on total line fluxes, and these observations in general cover too small a fraction of the galaxy as a whole to be useful here. Rosa-González, Terlevich, & Terlevich (2002) have assembled small-aperture emission-line fluxes for a set of 31 nearby star-forming galaxies, combined them with FIR fluxes from *IRAS*, and intercompared the results of applying the various diagnostics. With respect to SFR(FIR), which measures the total SFR, they find, with no extinction or inclination corrections, $\mathrm{SFR(FIR)} = 3.4\mathrm{SFR}(\mathrm{H}\alpha)$, with a large scatter (equivalent to ± 0.5 dex), and $\mathrm{SFR(FIR)} = 6.0\mathrm{SFR}(3727)$, with a dispersion equivalent to ± 0.8 dex. Because we are using inclination corrections, our dispersions should be and are somewhat smaller. We will compare these relations to those we use in the next section.

4. THE RATE OF STAR FORMATION VERSUS X-RAY FLUX IN THE HDF

As reviewed by Kennicutt (1998), there are many diagnostics that can be used to infer SFRs, ranging from continuum emission in the UV, far-IR, and radio to recombination and forbidden emission line strengths. The systematic errors induced by dust in several of these relations were discussed by Bell (2002), while Buat et al. (2002) discusses some of the problems associated with dust extinction in the UV and the use of UV fluxes, commonly used for galaxies with $z > 2.5$, where the rest-frame UV is redshifted into the optical band.

Given the wavelength coverage of the optical spectra from the CFGRS and the range of redshift under consideration, the SFRs for the distant galaxies in our sample in the region of the HDF can only be determined via the flux in the 3727 Å emission line of [O II], which is one of the less robust of these diagnostics. The strength of emission in this line is affected not only by dust but also, potentially, by variation of O excitation and the O abundance among the galaxies. The latter has been explored for local galaxies by Jansen et al. (2001) and at intermediate redshifts by Cardiel et al. (2003). All of these diagnostics are affected, each weighting a slightly different mass range, by the value of the initial mass function.

We measure the equivalent width in the 3727 Å doublet, which is not generally resolved in these spectra, in the observed frame, then transform that to the rest frame. SED parameters defined by the SED model of Cohen (2001) have been determined by Cohen (2001) for each of these galaxies from multicolor broadband photometry extending from U to K. These are used to interpolate within the set of observed broadband colors, yielding the continuum flux at rest-frame 3727 Å. Since the redshifts are known, the observed fluxes in the emission line are transformed into emitted luminosity in this emission line for each galaxy in the sample. We are forced to do this because the LRIS spectra are not fluxed; multislit spectra cannot in general be fluxed because of differential slit losses between objects observed, depending on the accuracy of the slit-mask alignment and of the astrometry used to design the slit masks. The adopted method of calculating the rest-frame equivalent width of an emission line assumes either that the line emission more or less follows the same spatial distribution as the background light of the galaxy or that the $1''$ wide slit used for the spectroscopy includes most of the total light of the galaxy. The latter is a reasonable assumption at the upper end of this redshift range; at $z = 0.8$, $1''$ corresponds to 7.3 kpc; the full size of the galaxy is sampled in the direction of the length of the slit.

The SFR is computed from the emitted flux in the [O II] line using the calibration of Kennicutt (1998). No corrections for internal extinction within the galaxies are made. The Galactic extinction in the direction of the HDF is very small and is ignored here. We do, however, correct for inclination of the galaxies, which does not remove the reddening experienced by a face-on disk galaxy. We measured rough axis ratios from the images of the flanking field galaxies obtained by the GOODS project (Giavalisco et al. 2003) and used the original HDF images for those galaxies within the HDF itself. Images taken in the F814W filter, the reddest used in both these *Hubble Space Telescope* (*HST*) surveys, were utilized when available. In a few cases, no *HST* image that was deep enough to indicate the shape of the outer isophotes of the galaxy could be located; no inclination correction was applied in such cases. We apply a correction of the form $\Delta(\mathrm{mag}) = \gamma \log(b/a)$. We assume $\gamma(3727) = 1.9$ mag, extrapolated from the work of Tully et al. (1998); this may be an underestimate of γ, which is rarely determined at wavelengths bluer than B. The SFR thus determined is denoted $SFR^i(3727)$.

There are two galaxies in the HDF sample with $z < 0.2$ for which the equivalent width of Hα is available from the CFGRS spectra. These, corrected for the inclusion of [N II] in the blend and for inclination effects as described above, yield $SFR^i(\mathrm{H}\alpha)$ in reasonable agreement with $SFR^i(3727)$. These galaxies both are of low luminosity; the volume of the cone of the CFGRS redshift survey at such low z is small. One of these is the object with the lowest SFR in this HDF sample, F36332_1134. The diagnostic ratio of Veilleux &

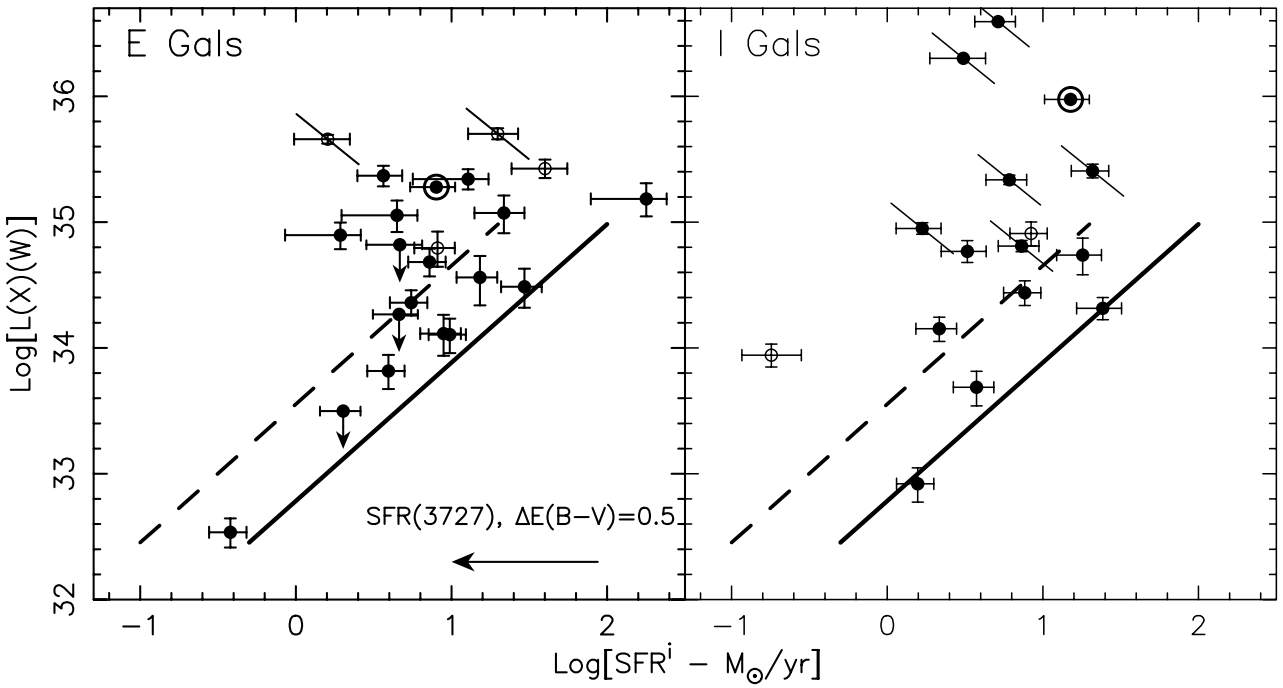

FIG. 4.—Total X-ray luminosity over the full *Chandra* band as a function of the SFR deduced from the luminosity in the 3727 Å emission line of [O II] and corrected for inclination effects, for the 22 $\mathscr{E}$ galaxies (*left*) and the 16 $\mathscr{I}$ galaxies (*right*). Open circles indicate galaxies lacking inclination corrections. The two suspected AGNs isolated from Fig. 1 are circled. The additional suspected AGNs isolated from Fig. 2 are marked with short diagonal lines. The least-squares linear fit to the local sample when Hα is used as the diagnostic for SFR is indicated as the thick solid line, while the dashed line denotes that expected from the 3727 Å emission line of [O II]. The arrow near the bottom of the left-hand panel denotes the decrease in SFR^i(3727) expected if $E(B-V)$ is increased by 0.5 mag.

Osterbrock (1987) indicates that light from H II regions dominates the optical emission lines.

The X-ray luminosity is taken directly from Alexander et al. (2003); the observed flux over the full *Chandra* bandpass is transformed into an emitted flux. Many of these sources are quite weak (see Fig. 2), and in some cases the X-ray spectral index could not be determined from the *Chandra* data. In a few cases, Alexander et al. (2003) tabulate only an upper limit to the total flux over the full *Chandra* band, presumably because of nondetection of the weakest sources in the higher frequency part of the *Chandra* bandpass. We therefore ignore any k-correction to the X-ray luminosity.

The resulting parameters for each galaxy in the CFGRS matched to within 1.″5 to a *Chandra* point source that shows evidence of strong current star formation from its optical spectrum are listed in Table 1 and displayed in Figure 4. The final sample contains 22 $\mathscr{E}$ galaxies and 16 $\mathscr{I}$ galaxies in the region of the HDF. The median redshifts are $z = 0.84$ for the former and $z = 0.49$ for the latter; $\mathscr{I}$ galaxies are harder to identify at high redshift (Cohen et al. 2000). The two galaxies that are discrepant in Figure 1 and suspected of harboring AGNs are marked in Figure 4, as are the suspected AGNs isolated from Figure 2.

The range of SFR^i at a fixed L_X in Figure 4 is large, and it is noticeably larger if the inclination corrections are not used, while the uncertainties in the values of L_X are small. The differences in internal extinction from galaxy to galaxy after correction to face-on is the dominant contributor to the scatter in Figure 4. The effect of ignoring the X-ray k-correction is relatively small. The uncertainties in the 3727 Å equivalent-width measurements, given in Table 1, are in general small. The conversion to an emitted line flux may introduce errors at the 30% level (Cohen 2001). The effect on the SFR^i derived from the observed luminosity in the 3727 Å emission line of an increase in the internal extinction within a galaxy of $E(B-V) = 0.5$ mag is indicated by the horizontal arrow at the bottom right of the left-hand panel of Figure 4. Table 4 summarizes the expected sources of uncertainty and the contributions of each. Their sum, in quadrature, is in good agreement with the dispersion seen in Figure 4 of SFR^i(3727) for a given L_X. This table offers a sobering reminder of why SFR^i(Hα) is a more robust indicator of SFR than is SFR^i(3727), but our options are limited.

Overall, aside from the suspected AGNs, the HDF galaxies display a relationship between L_X and SFR^i in Figure 4 that is highly reminiscent of that of the local calibrators, with larger scatter. The only major outlier among the $\mathscr{I}$ galaxies in the right-hand panel is a galaxy without an inclination correction. The $\mathscr{E}$ galaxies, shown in the left-hand panel, now show a tight relationship at low L_X. At the highest X-ray luminosities, the scatter is somewhat larger, while the three most luminous among the $\mathscr{E}$ galaxies and the five most luminous among the $\mathscr{I}$ galaxies are all suspected AGNs. It should also be noted that two of these $\mathscr{E}$ galaxies with L_X above that of the suspected AGNs and similar SFRs, F36348_1628 and F36246_1111, are not detected in the VLA radio surveys of Richards et al. (1998) and Richards (2000). Since they are both more distant than the suspected AGNs, that does not contradict the strong suggestion from Figure 2 that these are AGNs.

Table 2 lists the median properties of the samples in the region of the HDF, as well as those of the local comparison galaxies. The second-largest value for a given parameter

TABLE 5
SECOND-HIGHEST VALUE OF SAMPLES

Sample	Galaxies	SFR(Hα) ($M_\odot$ yr^{-1})	SFR(3727) ($M_\odot$ yr^{-1})	log M[a] ($M_\odot$)	SFR/10^{11} $M_\odot$(Hα) ($M_\odot$ yr^{-1})	SFR/10^{11} $M_\odot$(3727) ($M_\odot$ yr^{-1})
HDF Sample						
X-ray+radio+CFGRS[b]	11	...	29.4	11.55	...	36.7
X-ray+CFGRS/$\mathscr{E}$	22	...	39.9	11.41	...	83.2
X-ray+CFGRS/$\mathscr{I}$	16	...	29.4	11.55	...	14.3
Local Galaxies						
Local calibrators	14	53.7	...	11.15	40.5	...

[a] Log of the stellar mass inferred from the luminosity at rest-frame K.
[b] Only galaxies with optical emission lines are included.

among the galaxies in a particular sample is listed in Table 5. (We ignore the highest value to avoid outliers.) The SFR^i(3727) and SFR^i(Hα) are given for a face-on galaxy with no extinction correction.

If we wish to determine the total SFR, we need to evaluate $\Delta(A)$, the differential absorption between Hα and 3727 Å, and also A(Hα). For the reddening curve adopted here, the former is given by $\Delta(A) = 2.26E(B-V)$ mag, with $0 < \Delta(A)$, and almost certainly $\Delta(A) < 1.7$ mag. The second factor is given by $2.67E(B-V)$. Then

$$\mathrm{SFR(total)} = A(\mathrm{H}\alpha)\mathrm{SFR}^i(\mathrm{H}\alpha) ,$$

or

$$A(\mathrm{H}\alpha)\Delta(A)\mathrm{SFR}^i(3727) .$$

If we assume a typical A_V of 1.5 mag for star-forming galaxies, then

$$\mathrm{SFR(total)} = 2.7\mathrm{SFR}^i(\mathrm{H}\alpha) = 9.0\mathrm{SFR}^i(3727) .$$

Recognizing that their uncertainty is large, we adopt these values hereafter as typical for both the local and the HDF samples. The comparable relations obtained for 31 local galaxies by Rosa-González et al. (2002) have constants within 30% of those given above when either Hα or the 3727 Å emission line of [O II] is used as the SFR diagnostic.

5. COMPARISON OF THE SFRs BETWEEN THE HDF AND LOCAL SAMPLES

We have used the rest-frame K luminosity to infer the mass of each galaxy. We follow the procedure of Cohen (2001), where the SED parameters for each of the HDF galaxies are determined to deduce their rest-frame K luminosity, a procedure identical in principle to that described in § 4 and used to determine the continuum flux at rest-frame 3727 Å. These are the stellar masses; gas is not included. Masses have been deduced for each of the local calibrators using their integrated K flux from 2MASS (Skrutskie et al. 1997). The median mass of the local sample is 2.4×10^{10} $M_\odot$, comparable to that of the $\mathscr{E}$ galaxies in the HDF, while that of the $\mathscr{I}$ galaxies is ~3 times larger. As the range of galaxy masses is large, we compare the values of SFR$^i/10^{11}$ $M_\odot$ for the local sample and the HDF. These, plotted as a function of mass, are shown in Figures 5 and 6, respectively, while the medians and the second-highest values are given in Tables 2 and 5. Recall that for the local sample we use SFR^i(Hα), while for the HDF sample we use SFR^i(3727).

The parameter SFR$^i/10^{11}$ $M_\odot$ spans a range of a factor of ~100 for the HDF sample, which we regard as an indication of the rather broad galaxy spectral types used here, the lack of any luminosity indicator in the optical spectra, and our inability to differentiate $\mathscr{I}$ galaxies from $\mathscr{E}$ galaxies at $z \sim 1$. The $\mathscr{E}$ galaxy with the highest SFR$^i/10^{11}$ $M_\odot$ shown in Figure 6 is the highest redshift galaxy in our HDF sample, with $z = 1.355$. Its spectrum has been checked; the [O II] line strength and its errors appear valid. This galaxy is not discrepant in the L_X-SFR relationship of Figure 4. It appears to be a genuine case of a high-redshift galaxy with a very high SFR for its mass.

With no correction for reddening, Table 2 shows that the median SFR$^i/10^{11}$ $M_\odot$ for the $\mathscr{E}$ galaxies in the HDF is 2.6 times larger than that of the local galaxies, while that for the

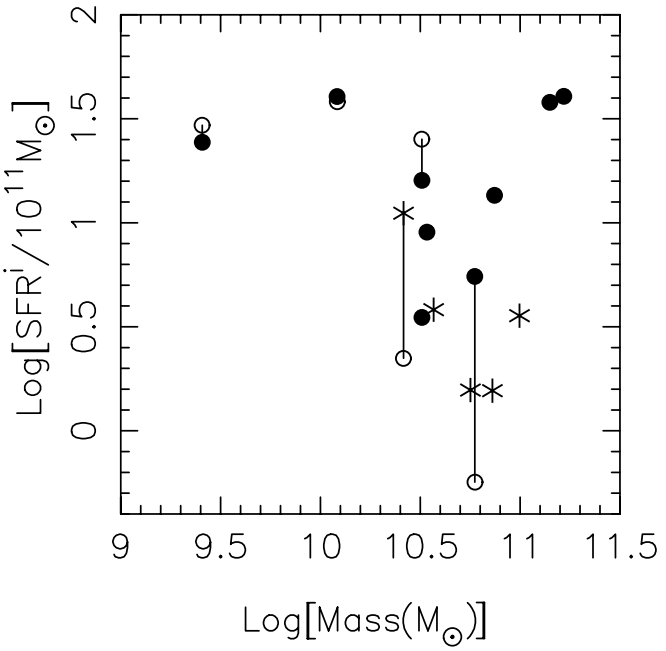

FIG. 5.—SFR^i(Hα)/10^{11} $M_\odot$ as a function of galaxy mass for the 14 galaxies in the local sample. Filled circles represent SFRs derived from Hα luminosities for galaxies with $(B-V)_0 < 0.6$, asterisks those of the redder star-forming galaxies, and open circles those using the 3727 Å line of [O II] as a diagnostic. Vertical lines connect the Hα and [O II] measurements, when both are available.

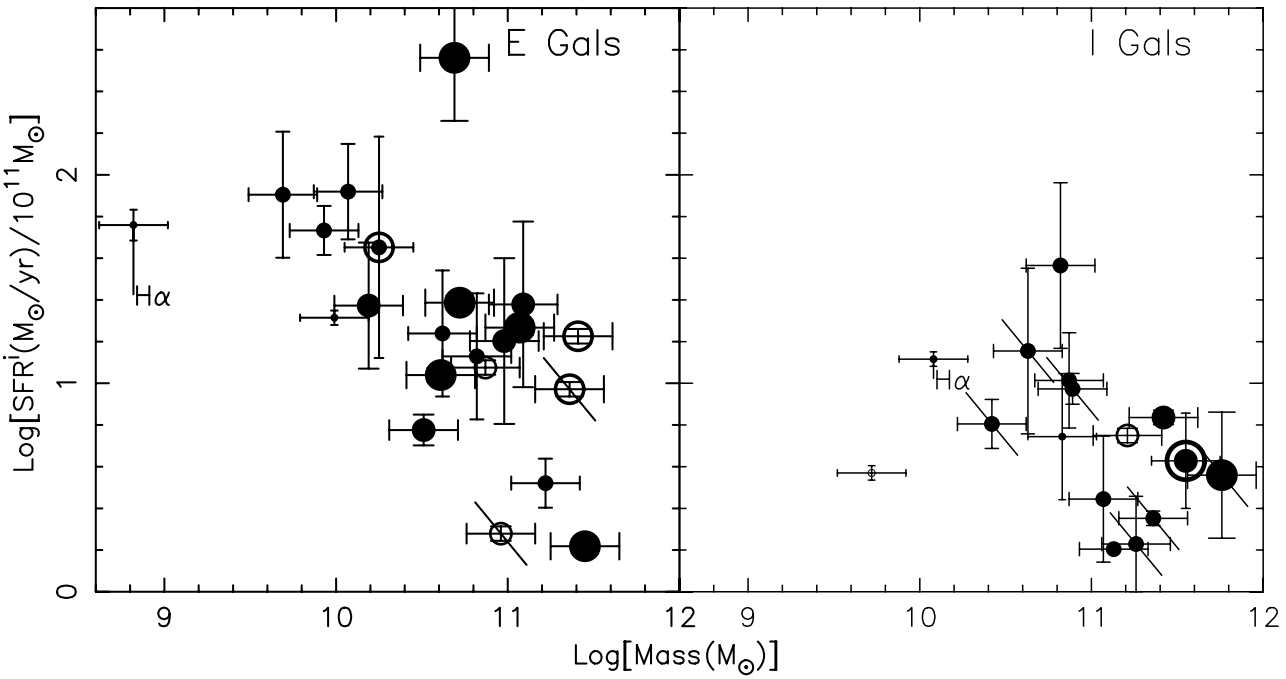

FIG. 6.—$SFR^i/10^{11}\ M_\odot$ as a function of the galaxy mass for the 22 $\mathscr{E}$ galaxies (*left*) and the 16 $\mathscr{I}$ galaxies (*right*). Galaxies without inclination corrections are shown as open circles. The symbol size indicates the redshift of the galaxy: from smallest to largest, $z < 0.35$, $0.35 < z < 0.7$, $0.7 < z < 1.0$, and $z > 1.0$. The two AGNs isolated from Fig. 1 are circled, while the additional suspected AGNs isolated from Fig. 2 are indicated by diagonal lines. The positions of the two galaxies with measured SFR(Hα) are indicated.

$\mathscr{I}$ galaxies is larger by a factor of 1.9. Thus, irrespective of the exact value of the two correction factors discussed above, the total SFR for the HDF galaxies is considerably larger than that of local galaxies. We adopt the nominal correction factors given above, with the additional support provided by the rough agreement with the local sample of Rosa-González et al. (2002). The median total SFR is then 7 times larger in the HDF sample than in the local galaxies. The median SFR per unit mass, $SFR^i/10^{11}\ M_\odot$, a measure of the efficiency of SFR, for the HDF is $\sim$1.7 times that for the local sample, with no extinction corrections. Applying the nominal extinction corrections suggests that the median SFR per unit mass is 5 times higher in the HDF.

We reject the suggestion that these differences arise from sample selection, such that only galaxies with very high SFRs can be detected at high redshift. Sample selection in the form of the incompleteness of the CFGRS is not believed to be a serious concern here. We see many galaxies in the HDF with SFRs lower (see Fig. 9) than those in the *Chandra* sample, at least for $z < 1.1$. In this context, we note that the CFGRS could have detected emission in the 3727 Å line at least 5 times smaller than that observed for F36527_1355 at $z = 1.355$.

In local galaxies, a simple Schmidt (1959) power law accurately relates a galaxy's total SFR to its disk-averaged gas surface density. However, we do not know the gas density in these systems, and information on possible mergers is not available either, so we cannot attempt to isolate the additional factors beyond total stellar mass that undoubtedly influence the SFR in a particular galaxy.

In spite of these concerns, the similar form of the relationship between L_X, SFR^i, L_{radio}, and L_{FIR} in HDF samples of varying sizes, once cleaned of AGNs and taking reddening into consideration (for SFR only), presented here, by Grimm et al. (2003), and by Garrett (2002), suggests that the physical mechanism for star formation is similar among all the galaxies discussed here and that it is operating in more or less the same way, but galaxies of higher mass dominate the star formation in the HDF, while lower mass galaxies dominate the star formation locally, as was already pointed out by Cowie et al. (1996) and others.

5.1. *Constraints on the SFR at Still Higher Redshift*

We consider whether the present SFR in each galaxy in the HDF sample is consistent with its age as inferred from its redshift z or whether the time-averaged SFR had to be even higher in the past to have formed the observed mass of stars. This provides a window into the behavior of SFR with z (Madau, Pozzetti, & Dickinson 1998) in a redshift regime in which observations are more difficult. Figure 7 shows $SFR^i(3727)$ for the HDF sample as a function of galaxy mass. The thick solid line indicates the accumulated stellar mass of a galaxy after 6×10^9 yr (the age of a $z \sim 1$ galaxy) for an SFR constant with time. If a galaxy is located to the right of the line, there has been insufficient time to produce the observed stellar content of the galaxy, assuming an SFR constant with time. In such a case, the time-averaged SFR must have been higher in the past (i.e., presumably at z between 1 and 2, as the total age at $z > 2$ is very small, $\lesssim$1 Gyr).

The symbol size in Figure 7 increases with redshift, so we check whether the galaxies with $z > 0.7$ are systematically to the right of the line. The $\mathscr{E}$ galaxies are distributed fairly close to this line, while the $\mathscr{I}$ galaxies tend to be to the right of it. Their median redshift is half that of the $\mathscr{E}$ galaxies (Table 2), but the dashed line in the right-hand panel of the figure indicates the mass expected for constant SFR and an age of 9 Gyr; the $\mathscr{I}$ galaxies still tend to lie to the right of that.

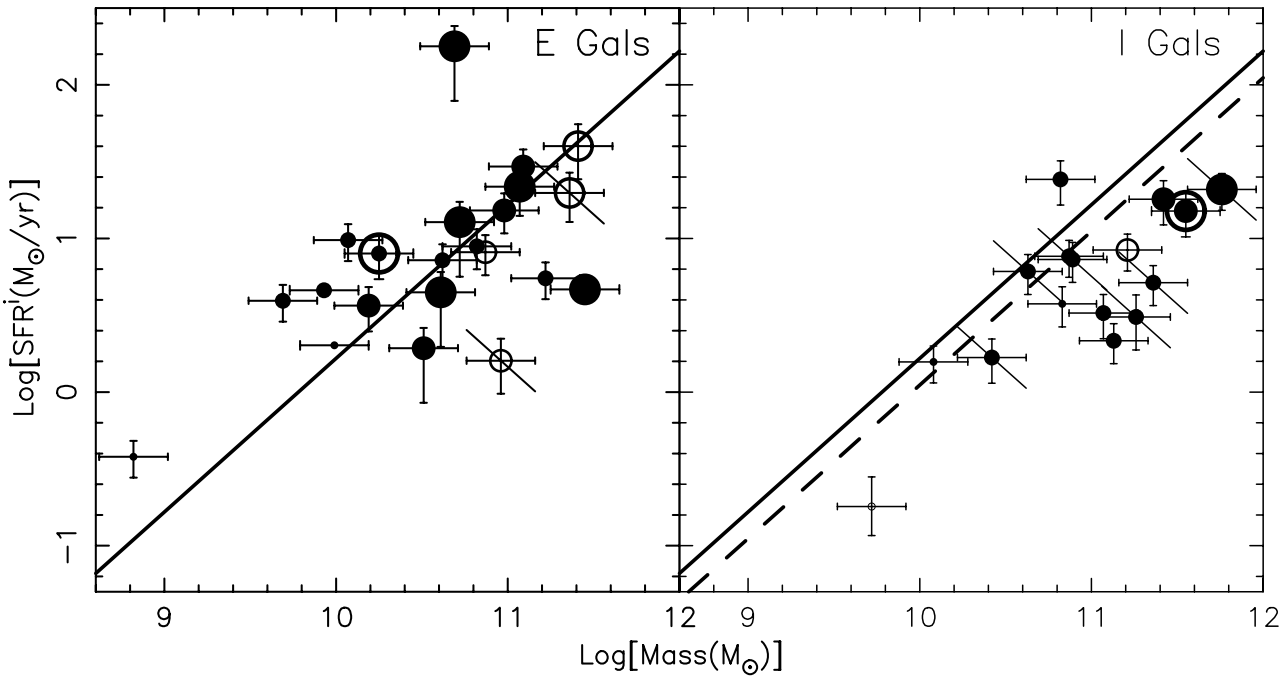

FIG. 7.—SFR^i(3727) for the sample of X-ray–emitting galaxies in the region of the HDF as a function of galaxy stellar mass: the 16 $\mathscr{I}$ galaxies (*right*) and the 22 $\mathscr{E}$ galaxies (*left*). The symbol size indicates the redshift of the galaxy, as in Fig. 6. Open circles indicate galaxies lacking measured axis ratios. The two AGNs isolated from Fig. 1 are circled, while the additional suspected AGNs isolated from Fig. 2 are indicated by short diagonal lines. The thick solid line denotes the mass in stars achieved as function of SFR^i after 6×10^9 yr, assuming constant SFR with time. The dashed line in the right-hand panel is for an elapsed time of 9 Gyr.

For the $\mathscr{E}$ galaxies in the HDF, only one high-redshift galaxy appears to be more than a factor of 3 from the line. This case, and the smaller offsets to the right of the line of the other $z \sim 1$ galaxies, can easily be accommodated by the factors $\Delta(A)$ and $A(\mathrm{H}\alpha)$, both assumed to be unity here, as well as by a few missing inclination corrections. So there is no need for a substantially higher SFR at $z > 1$ to produce the stars seen in galaxies at $z \sim 1$. The current SFR at $z \sim 1$ is consistent with the time-averaged SFR for $z > 1$ for the $\mathscr{E}$ galaxies. It is possible, but not demonstrated here, that the absorption corrections $A(\mathrm{H}\alpha)\Delta(A)$ can also produce consistency for the $\mathscr{I}$ galaxies without requiring a higher time-averaged SFR in the past. Further tests of this, once more data become available, will be interesting.

6. THE ORIGIN OF THE X-RAY EMISSION FROM THESE GALAXIES

We now consider which star-forming galaxies within the HDF show X-ray emission. Cohen (2003) presents rest-frame equivalent widths for the 3727 Å emission line of [O II] in a sample of 256 galaxies from the CFGRS in the region of the HDF. Figure 8 shows these as a function of redshift, with the X-ray–luminous objects of the present sample indicated by larger symbols. We see that the X-ray–luminous objects are not, in general, those galaxies at a given z with the largest equivalent widths but are mixed through the entire range of equivalent width, with a concentration toward the lower values. However, the equivalent width is not a measure of the emitted luminosity in the line. When we plot instead the emitted luminosity in the [O II] emission line at 3727 Å (see Fig. 9) versus redshift, the situation is somewhat clearer. The X-ray–luminous galaxies are among the most luminous in the full HDF sample of the CFGRS in this emission line; i.e., they have among the highest SFRs at each z, but having a very high SFR does not guarantee that a galaxy will be detected in the *Chandra*

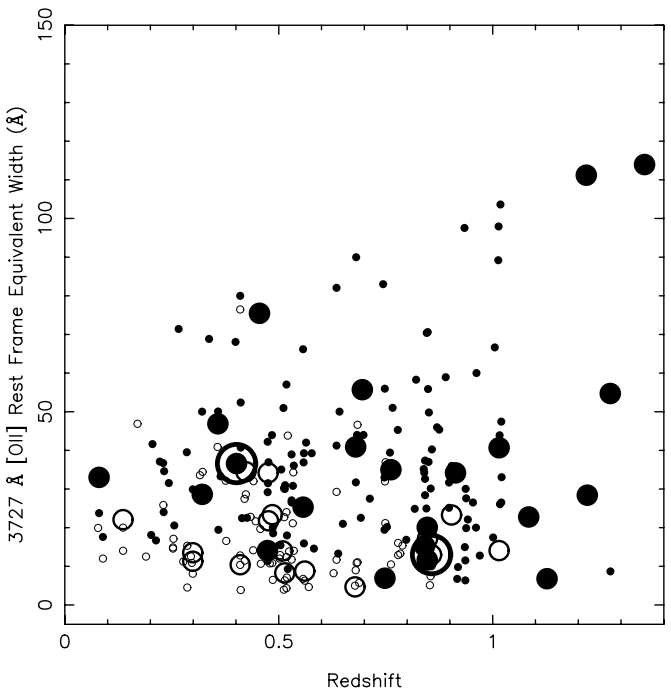

FIG. 8.—Rest-frame equivalent width of the 3727 Å emission line of [O II] for a sample of ~200 star-forming galaxies in the region of the HDF from Cohen (2003), ignoring a few broad-lined AGNs. Open circles indicate $\mathscr{I}$ galaxies, while filled circles indicate $\mathscr{E}$ galaxies. The X-ray–emitting galaxies are marked by larger symbols. The two suspected AGNs are circled.

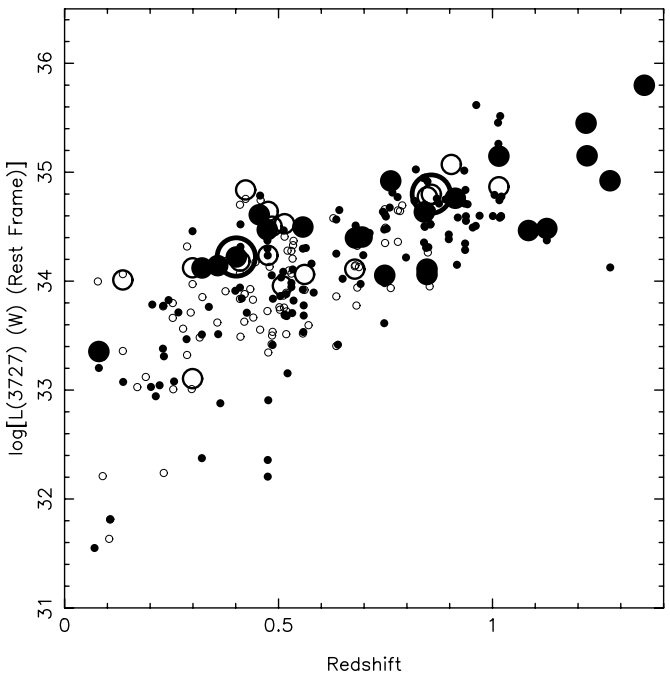

FIG. 9.—Emitted luminosity in the rest frame in the 3727 Å emission line of [O II] for the sample used in Fig. 8. Open circles indicate $\mathscr{I}$ galaxies while filled circles indicate $\mathscr{E}$ galaxies. The X-ray–emitting galaxies are marked by larger symbols. The two suspected AGNs are circled. No inclination corrections have been made.

images. We cannot at present isolate the additional factors beyond the mass of a galaxy that might influence its SFR at $z \sim 1$.

However, Figure 2 offers some possible clues. We suggest that the small number of discrepant galaxies in this figure all have weak nuclear AGNs. We suggest that the normal star-forming galaxies are those sprinkled along the bottom of this figure. These all have very low full-band *Chandra* counts, almost all less than 20 full-band counts. This is right at the detection limit of even the 2 Ms *Chandra* image (Alexander et al. 2003). The small variations in inclination angle and reddening mean that those galaxies with the maximum detected 3727 Å line flux at any given redshift (i.e., the upper envelope of the distribution in Fig. 9) can only suggest, but not define, the set of galaxies with the highest total SFRs. The lack of *Chandra* detection of galaxies with SFRs apparently slightly higher or comparable to those detected becomes a matter of chance, the inclination, or the reddening. The spatial position of the galaxy within the *Chandra* field, in particular its distance from the center of the *Chandra* field (where detection limits are higher), may also play a role. With this hypothesis to explain why some star-forming galaxies we would expect to have been detected by *Chandra* are not, the L_X-SFR relation among the star-forming galaxies in the region of the HDF becomes indistinguishable from that of local galaxies, and $L_X \propto$ SFR.

7. SUMMARY

There have been many efforts to determine the SFR at high redshift. The evolution with redshift of the rest-frame UV luminosity density was used by, among others, Lilly et al. (1996), Cohen (2002), and Wilson et al. (2002) to study the evolution of the SFR with z, while Hogg et al. (1998) used the evolution of the [O II] luminosity density for the same purpose. All agree on a strong increase in these SFR diagnostics between the local universe and $z \sim 1$. In the present analysis, we see this manifested through the emission-line strengths of individual galaxies; the very high emitted luminosity in the 3727 Å line of [O II] and the inferred SFRs found among the most extreme galaxies in the HDF sample (see Tables 1 and 2) surpass anything seen in the local universe. The enhancement in SFR per unit galaxy mass is also substantial.

A comparison of the X-ray, radio, and optical data suggests (Figs. 1 and 2), in agreement with evidence from other surveys, that ~20% of the X-ray sources contain weak AGNs, even though these galaxies (ignoring the two broad-lined AGNs that have been deleted from the HDF sample) appear from optical spectra of their integrated light to be "normal." Aperture effects appear to limit our ability to detect AGNs from such spectra in high-redshift samples, as suggested by Moran et al. (2002). These AGNs produce more than 90% of the detected *Chandra* flux arising from objects in the redshift regime $0.4 \lesssim z < 1.1$.

Because we are using the 3727 Å emission line of [O II] as our diagnostic of SFR, reddening is a serious concern, and we found that the introduction of inclination corrections significantly reduced the scatter in the L_X-SFR relation. This is the first detection, to our knowledge, of inclination effects in such distant galaxies. It is very likely that inclination effects also contribute to the distribution of SEDs among distant star-forming galaxies. They probably cause a significant part of the spread observed in the SED parameters α_{UV} and T(sBB) determined by Cohen (2001) for the sets of $\mathscr{I}$ and $\mathscr{E}$ galaxies in the region of the HDF.

Once the reddening corrections are incorporated and the AGNs eliminated, we suggest that the L_X-SFR relation for these distant galaxies is essentially identical to that prevailing in local star-forming galaxies. The L_X-radio relation, presented here and, for a smaller sample, by Grimm et al. (2003), and the L_X-FIR relation of Garrett (2002) for the HDF both agree with those of local star-forming galaxies. This suggests that the physical mechanisms responsible for X-ray emission in these distant galaxies are the same as those that act locally.

High observed flux in the 3727 Å line of [O II] is a necessary but not sufficient condition for detection by *Chandra*. The issue of which particular galaxies are detected by *Chandra* is resolved by realizing that the normal star-forming galaxies in our sample lie essentially at or only slightly above the *Chandra* detection limit. Inclination, reddening, etc., which affect the transformation from [O II] emission-line flux to total SFR, can lead to a particular galaxy being detected by *Chandra*, whereas another with similar SFR^i(3727) at the same redshift may not be detected.

Many optical surveys of distant galaxies are underway that plan to use 3727 Å emission as a diagnostic for SFR and metallicity. In qualitative terms, if the problems of internal reddening and potential AGN contribution can be handled, the emitted luminosity in the 3727 Å emission line does appear to be a reasonable indicator of the SFR among these distant galaxies, but this work illustrates the difficulties associated with this emission line, for which reddening is such a serious concern.

Once larger samples of distant galaxies with high-precision, multiwavelength data permitting the use of

multiple diagnostics for their SFRs become available, one might be able to explore the issue of the constancy of the initial mass function between the local and the distant universe. The comparison we have carried out of the expected stellar mass, assuming constant SFR, with the actual galaxy stellar mass at $z \sim 1$ suggests that no further rise in time-averaged SFR is necessary at earlier times. Extending this to a larger sample with better data will be of considerable interest, as it probes the time-averaged SFR at a key epoch of the formation of galaxies.

The entire Keck/HIRES user community owes a huge debt to Jerry Nelson, Gerry Smith, Bev Oke, and many other people who have worked to make the Keck Telescope and LRIS a reality and to operate and maintain the Keck Observatory. We are grateful to the W. M. Keck Foundation for the vision to fund the construction of the W. M. Keck Observatory. The author extends special thanks to those of Hawaiian ancestry on whose sacred mountain we are privileged to be guests. Without their generous hospitality, none of the observations presented herein would have been possible. I am grateful to R. Sunyaev for helpful conversations and to my collaborators in the HDF-N redshift survey, in particular A. Phillips and Len Cowie, who provided in digital form spectra of several galaxies in the HDF. I thank the referee for helpful suggestions.

This publication makes use of data products from the 2MASS, which is a joint project of the University of Massachusetts and the Infrared Processing and Analysis Center/California Institute of Technology, funded by the National Aeronautics and Space Administration and by the National Science Foundation. This research has made use of the NASA/IPAC Extragalactic Database (NED), which is operated by the Jet Propulsion Laboratory, California Institute of Technology, under contract with the National Aeronautics and Space Administration. The extragalactic work of the author is not supported by any federal agency.

REFERENCES

Alexander, D. M., et al. 2003, AJ, 126, 539
Aussel, H., Cesarsky, C. J., Elbaz, D., & Starck, J. L. 1999, A&A, 342, 313
Baldwin, J. A., Phillips, M. M., & Terlevich, R. 1981, PASP, 93, 5
Barger, A. J., Cowie, L. L., Brandt, W. N., Capak, P., Garmire, G. P., Hornschemeier, A. E., Steffen, A. T., & Wehner, E. H. 2002, AJ, 124, 1839
Barger, A. J., Cowie, L. L., Capak, P., Alexander, D. M., Bauer, F. E., Brandt, W. N., Garmire, G. P., & Hornschemeier, A. E. 2003, ApJ, 584, L61
Bell, E. F. 2002, ApJ, 577, 150
———. 2003, ApJ, 586, 794
Bell, E. F., & Kennicutt, R. C., Jr. 2001, ApJ, 548, 681
Buat, V., Boselli, A., Gavazzi, G., & Bonfanti, C. 2002, A&A, 383, 801
Calzetti, D. 1999, Ap&SS, 266, 243
Calzetti, D., Bohlin, R. C., Kinney, A. L., Storchi-Bergmann, T., & Heckman, T. M. 1995, ApJ, 443, 136
Calzetti, D., Kinney, A. L., & Storchi-Bergmann, T. 1994, ApJ, 429, 582
Cardiel, N., Elbaz, D., Schiavon, R. P., Willmer, C. N. A., Koo, D. C., Phillips, A. C., & Gallego, J. 2003, ApJ, 584, 76
Cohen, J. G. 2001, AJ, 121, 2895
———. 2002, ApJ, 567, 672
———. 2003, in Rev. Mexicana Astron. Astrofis. Ser. Conf., Galaxy Evolution: Theory and Observations, ed. V. Avila-Reese, C. Firmani, C. Frenk, & C. Allen (Mexico: Inst. Astron., UNAM), in press
Cohen, J. G., Cowie, L. L., Hogg, D. W., Songaila, A., Blandford, R., Hu, E. M., & Shopbell, P. 1996, ApJ, 471, L5
Cohen, J. G., Hogg, D. W., Blandford, R., Cowie, L. L., Hu, E., Songaila, A., Shopbell, P., & Richberg, K. 2000, ApJ, 538, 29
Cohen, J. G., Hogg, D. W., Pahre, M. A., Blandford, R., Shopbell, P. L., & Richberg, K. 1999, ApJS, 120, 171
Condon, J. J. 1992, ARA&A, 30, 575
Cowie, L. L., Songaila, A., Hu, E. M., & Cohen, J. G. 1996, AJ, 112, 839
Fabbiano, G. 1989, ARA&A, 27, 87
Fabbiano, G., Kim, D.-W., & Trinchieri, G. 1992, ApJS, 80, 531
Fabbiano, G., Zezas, A., & Murray, S. S. 2001, ApJ, 554, 1035
Ferrarese, L., & Merritt, D. 2000, ApJ, 539, L9
Gallagher, J. S., Bushouse, H., & Hunter, D. A. 1989, AJ, 97, 700
Garrett, M. A. 2002, A&A, 384, L19
Giavalisco, M., et al. 2003, ApJL, 598
Grimm, H. J., Gilfanov, M., & Sunyaev, R. 2003, MNRAS, 339, 793
Ho, L. C., Filippenko, A. V., & Sargent, W. L. W. 1997, ApJ, 487, 568
Hogg, D. W., Cohen, J. G., Blandford, R., & Pahre, M. A. 1998, ApJ, 504, 622
Hogg, D. W., et al. 2000, ApJS, 127, 1
Hornschemeier, A. E., et al. 2003, AJ, 126, 575
Huchra, J., & Burg, R. 1992, ApJ, 393, 90
Immler, S., Pietsch, W., & Aschenbach, B. 1998, A&A, 331, 601
Jansen, R. A., Franx, M., & Fabricant, D. 2001, ApJ, 551, 825
Jarrett, T. H., Chester, T., Cutri, R., Schneider, S. E., & Huchra, J. P. 2003, AJ, 125, 525
Kauffmann, G., et al. 2003, MNRAS, 341, 54
Kennicutt, R. C., Jr. 1983, ApJ, 272, 54
———. 1992, ApJ, 388, 310
———. 1998, ARA&A, 36, 189
Kobulnicky, H. A., et al. 2003, ApJ, in press
Lilly, S. J., LeFèvre, O., Hammer, F., & Crampton, D. 1996, ApJ, 460, L1
Lira, P., Ward, M., Zezas, A., Alonso-Herrero, A., & Ueno, S. 2002, MNRAS, 330, 259
Madau, P., Pozzetti, L., & Dickinson, M. 1998, ApJ, 498, 106
Makishima, K., et al. 2000, ApJ, 535, 632
Martin, C. L., Kobulnicky, H. A., & Heckman, T. M. 2002, ApJ, 574, 663
McQuade, K., Calzetti, D., & Kinney, A. L. 1995, ApJS, 97, 331
Moran, E. C., Filippenko, A. V., & Chornock, R. 2002, ApJ, 579, L71
Moran, E. C., Lehnert, M. D., & Helfand, D. J. 1999, ApJ, 526, 649
Okada, K., Mitsuda, K., & Dotani, T. 1997, PASJ, 49, 653
Oke, J. B., et al. 1995, PASP, 107, 375
Phillips, A. C., Guzmán, R., Gallego, J., Koo, D. C., Lowenthal, J. D., Vogt, N. P., Faber, S. M., & Illingworth, G. D. 1997, ApJ, 489, 543
Ptak, A., & Griffiths, R. 1999, ApJ, 517, L85
Read, A. M., & Stevens, I. R. 2002, MNRAS, 335, L36
Richards, E. A. 2000, ApJ, 533, 611
Richards, E. A., Kellermann, K. I., Fomalont, E. B., Windhorst, R. A., & Partridge, R. B. 1998, AJ, 116, 1039
Rola, C. S., Terlevich, E., & Terlevich, R. J. 1997, MNRAS, 289, 419
Rosa-González, D., Terlevich, E., & Terlevich, R. 2002, MNRAS, 332, 283
Schlegel, D. J., Finkbeiner, D. P., & Davis, M. 1998, ApJ, 500, 525
Schmidt, M. 1959, ApJ, 129, 243
Skrutskie, M. F., et al. 1997, in The Impact of Large Scale Near-IR Sky Surveys, ed. F. Garzón, N. Epchtein, A. Omont, B. Burton, & P. Persi (Dordrecht: Kluwer), 25
Storchi-Bergmann, T., Kinney, A. L., & Challis, P. 1995, ApJS, 98, 103
Tenorio-Tagle, G., Silich, S. A., Kunth, D., Terlevich, E., & Terlevich, R. 1999, MNRAS, 309, 332
Terashima, Y., & Wilson, A. S. 2001, ApJ, 560, 139
———. 2003, ApJ, submitted (astro-ph/0305563)
Tully, R. B., Pierce, M. J., Huang, J.-S., Saunders, W., Verheijen, M. A. W., & Witchalls, P. L. 1998, AJ, 115, 2264
Ueda, Y., Ishisaki, T., Takahashi, T., Makishima, K., & Ohashi,T. 2001, ApJS, 133, 1
Veilleux, S., & Osterbrock, D. E. 1987, ApJS, 63, 295
Vogler, A., & Pietsch, W. 1997, A&A, 319, 459
Williams, R. E., et al. 1996, AJ, 112, 1335
Wilson, G., Cowie, L. L., Barger, A. J., & Burke, D. J. 2002, AJ, 124, 1258
Young, J. S., Allen, L., Kenney, J. D. P., Lesser, A., & Rownd, B. 1996, AJ, 112, 1903
Zezas, A., & Fabbiano, G. 2002, ApJ, 577, 726